

Front-End Electronics and Signal Processing

Helmuth Spieler

Lawrence Berkeley National Laboratory, Physics Division, Berkeley, CA 94720, U.S.A.

Abstract. Basic elements of front-end electronics and signal processing for radiation detectors are presented. The text covers system components, signal resolution, electronic noise and filtering, digitization, and some common pitfalls in practical systems.

INTRODUCTION

Electronics are a key component of all modern detector systems. Although experiments and their associated electronics can take very different forms, the basic principles of the electronic readout and optimization of signal-to-noise ratio are the same. This paper provides a summary of front-end electronics components and discusses signal processing with an emphasis on electronic noise. Because of space limitations, this can only be a brief overview. The full course notes are available as pdf files on the world wide web [1]. More detailed discussions on detectors, signal processing and electronics are also available on the web [2].

The purpose of pulse processing and analysis systems is to

1. Acquire an electrical signal from the sensor. Typically this is a short current pulse.
2. Tailor the time response of the system to optimize
 - a) the minimum detectable signal (detect hit/no hit),
 - b) energy measurement,
 - c) event rate,
 - d) time of arrival (timing measurement),
 - e) insensitivity to sensor pulse shape,or some combination of the above.
3. Digitize the signal and store for subsequent analysis.

Position-sensitive detectors utilize the presence of a hit, amplitude measurement or timing, so these detectors pose the same set of requirements. Generally, these properties cannot be optimized simultaneously, so compromises are necessary.

In addition to these primary functions of an electronic readout system, other considerations can be equally or even more important, for example, radiation resistance, low power (portable systems, large detector arrays, satellite systems), robustness, and – last, but not least – cost.

Example System

Fig. 1 illustrates the components and functions in a radiation detector using a scintillation detector as an example. Radiation – in this example gamma rays – is absorbed in a scintillating crystal, which produces visible light photons. The number of scintillation photons is proportional to the absorbed energy. The scintillation photons are detected by a photomultiplier (PMT), consisting of a photocathode and an

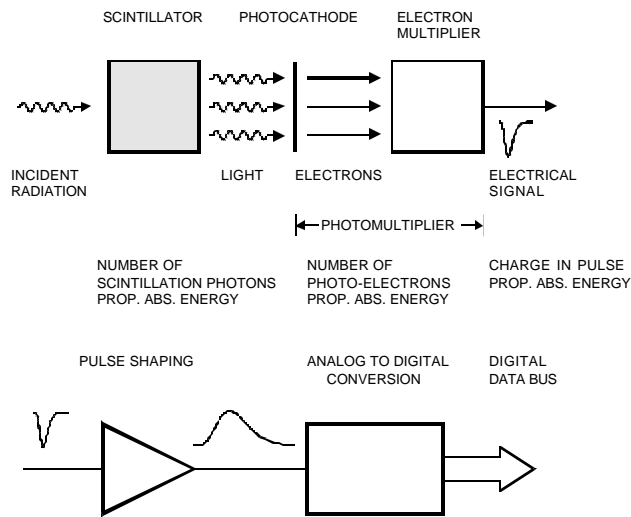


FIGURE 1. Example detector signal processing chain.

electron multiplier. Photons absorbed in the photocathode release electrons, where the number of electrons is proportional to the number of incident scintillation photons. At this point energy absorbed in the scintillator has been converted into an electrical signal whose charge is proportional to energy. The electron multiplier increases this signal charge by a constant factor. The signal at the PMT output is a current pulse. Integrated over time this pulse contains the signal charge, which is proportional to the absorbed energy. The signal now passes through a pulse shaper whose output feeds an analog-to-digital converter (ADC), which converts the analog signal into a bit-pattern suitable for subsequent digital storage and processing. If the pulse shape does not change with signal charge, the peak amplitude – the pulse height – is a measure of the signal charge, so this measurement is called pulse height analysis. The pulse shaper can serve multiple functions, which are discussed below. One is to tailor the pulse shape to the ADC. Since the ADC requires a finite time to acquire the signal, the input pulse may not be too short and it should have a gradually rounded peak. In scintillation detector systems it is frequently an integrator and implemented as the first stage of the ADC, so it is invisible to the casual observer. Then the system appears very simple, as the PMT output is plugged directly into a charge-sensing ADC.

Detection Limits and Resolution

The minimum detectable signal and the precision of the amplitude measurement are limited by fluctuations. The signal formed in the sensor fluctuates, even for a fixed

energy absorption. Generally, sensors convert absorbed energy into signal quanta. In the scintillation detector shown as an example above, absorbed energy is converted into a number of scintillation photons. In an ionization chamber, energy is converted into a number of charge pairs (electrons and ions in gases or electrons and holes in solids). The absorbed energy divided by the excitation energy yields the number of signal quanta $N = E/e_i$.

This number fluctuates statistically, so the relative resolution

$$\frac{\Delta E}{E} = \frac{\Delta N}{N} = \frac{\sqrt{FN}}{N} = \sqrt{\frac{F e_i}{E}}.$$

The resolution improves with the square root of energy. F is the Fano factor, which comes about because multiple excitation mechanisms can come into play and reduce the overall statistical spread. For example, in a semiconductor absorbed energy forms electron-hole pairs, but also excites lattice vibrations – quantized as phonons – whose excitation energy is much smaller (meV vs. eV). Thus many more excitations are involved than apparent from the charge signal alone and this reduces the statistical fluctuations of the charge signal. For example, in Si the Fano factor is 0.1.

In addition, electronic noise introduces baseline fluctuations, which are superimposed on the signal and alter the peak amplitude. Fig. 2 (left) shows a typical noise waveform. Both the amplitude and time distributions are random.

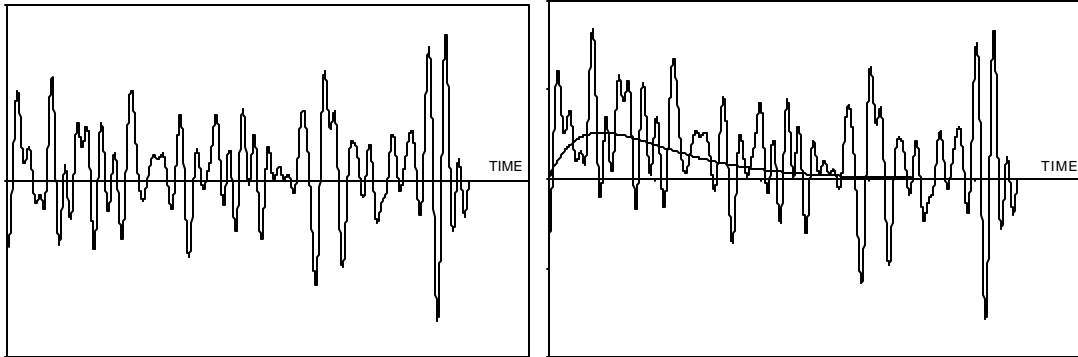


FIGURE 2. Waveform of random noise (left) and signal + noise (right), where the peak signal is equal to the r.m.s. noise level ($S/N = 1$). The noiseless signal is shown for comparison.

When superimposed on a signal, the noise alters the both the amplitude and time dependence. Fig. 2 (right) shows the noise waveform superimposed on a small signal. As can be seen, the noise level determines the minimum signal whose presence can be discerned.

In an optimized system, the time scale of the fluctuations is comparable to that of the signal, so the peak amplitude fluctuates randomly above and below the average value. This is illustrated in Fig. 3, which shows the same signal viewed at four different times. The fluctuations in peak amplitude are obvious, but the effect of noise on timing measurements can also be seen. If the timing signal is derived from a threshold discriminator, where the output fires when the signal crosses a fixed threshold, amplitude fluctuations in the leading edge translate into time shifts. If one derives the time of arrival from a centroid analysis, the timing signal also shifts (compare the top and bottom right figures). From this one sees that signal-to-noise

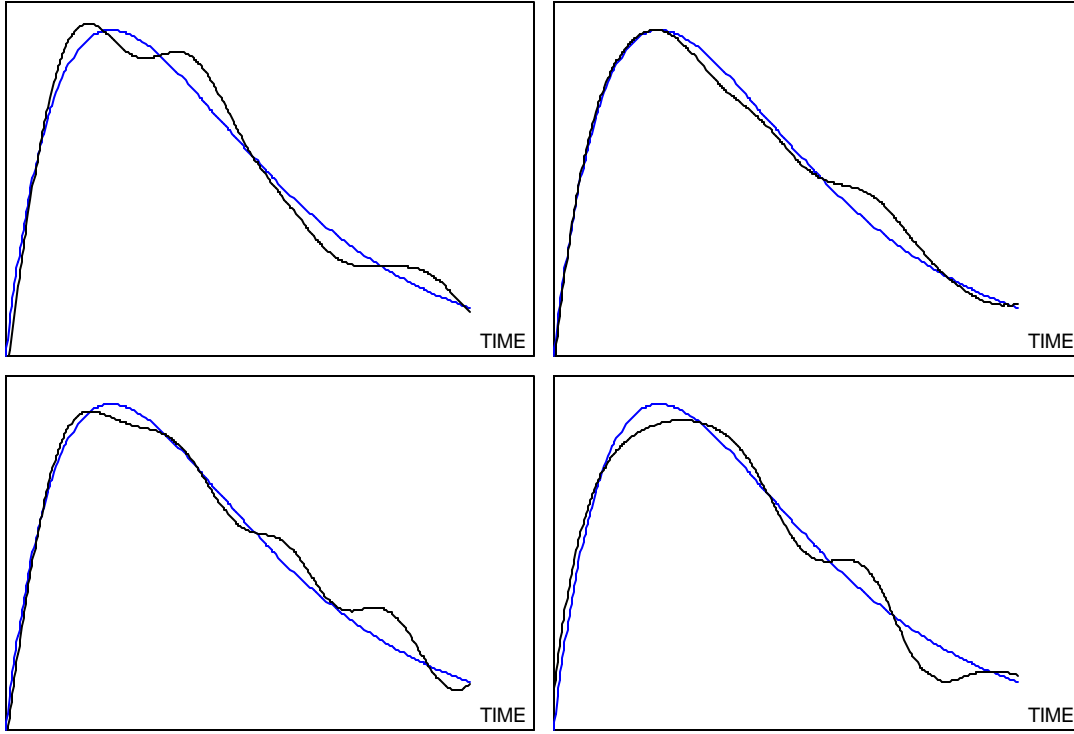


FIGURE 3. Signal plus noise at four different times. The noiseless signal is superimposed for comparison.

ratio is important for all measurements – sensing the presence of a signal or the measurement of energy, timing, or position.

ACQUIRING THE SENSOR SIGNAL

The sensor signal is usually a short current pulse $i_s(t)$. Typical durations vary widely, from 100 ps for thin Si sensors to tens of μ s for inorganic scintillators. However, the physical quantity of interest is the deposited energy, so one has to integrate over the current pulse

$$E \propto Q_s = \int i_s(t) dt .$$

This integration can be performed at any stage of a linear system, so one can

1. integrate on the sensor capacitance,
2. use an integrating preamplifier (“charge-sensitive” amplifier),
3. amplify the current pulse and use an integrating ADC (“charge sensing” ADC),
4. rapidly sample and digitize the current pulse and integrate numerically.

In high-energy physics the first three options tend to be most efficient.

Signal Integration

Fig. 4 illustrates signal formation of an ionization chamber connected to an amplifier with a very high input resistance. The ionization chamber volume could be filled with gas or a solid, as in a silicon sensor. As mobile charge carriers move towards their respective electrodes they change the induced charge on the sensor electrodes, which form a capacitor C_{det} . If the amplifier has a very small input resistance R_i , the time constant $\tau = R_i(C_{det} + C_i)$ for discharging the sensor is small, and the amplifier will sense the signal current. However, if the input time constant is large compared to the duration of the current pulse, the resulting voltage at the amplifier input

$$V_{in} = \frac{Q_s}{C_{det} + C_i}.$$

The magnitude of the signal is dependent on the sensor capacitance. In a system with varying sensor capacitances, a Si tracker with varying strip lengths, for example, or a partially depleted semiconductor sensor, where the capacitance varies with the applied bias voltage, one would have to deal with additional calibrations. Although this is possible, it is awkward, so it is desirable to use a system where the charge calibration is independent of sensor parameters. This can be achieved rather simply with a charge-sensitive amplifier.

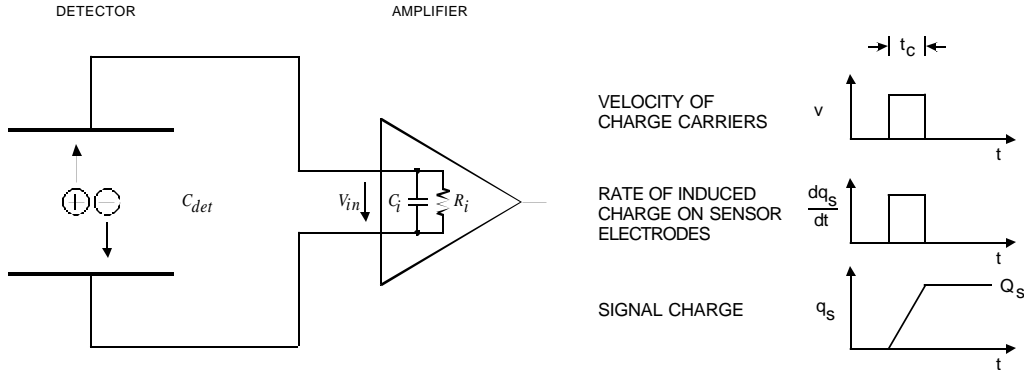


Figure 4. Charge collection and signal integration in an ionization chamber

Fig. 5 shows the principle of a feedback amplifier that performs integration. It consists of an inverting amplifier with voltage gain $-A$ and a feedback capacitor C_f connected from the output to the input. To simplify the calculation, let the amplifier have infinite input impedance, so no current flows into the amplifier input. If an input signal produces a voltage v_i at the amplifier input, the voltage at the amplifier output is $-Av_i$. Thus, the voltage difference across the feedback capacitor $v_f = (A + 1)v_i$ and the charge deposited on C_f is $Q_f = C_f v_f = C_f(A + 1)v_i$. Since no current can flow into the amplifier, all of the signal current must charge up the feedback capacitance, so $Q_f = Q_i$. The amplifier input appears as a “dynamic” input capacitance

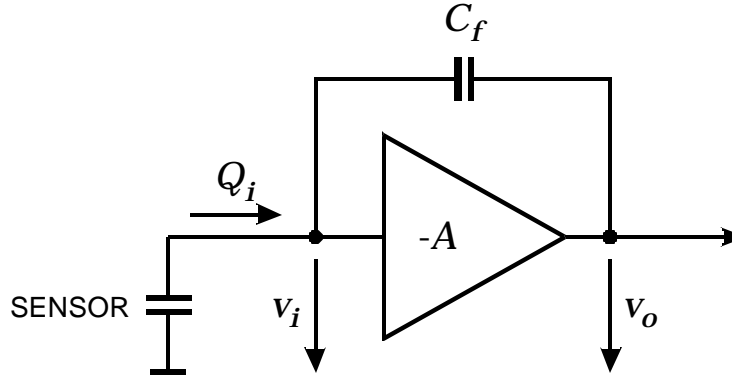


FIGURE 5. Basic configuration of a charge-sensitive amplifier

$$C_i = \frac{Q_i}{v_i} = C_f(A+1).$$

The voltage output per unit input charge

$$A_Q = \frac{dv_o}{dQ_i} = \frac{Av_i}{C_i v_i} = \frac{A}{C_i} = \frac{A}{A+1} \cdot \frac{1}{C_f} \approx \frac{1}{C_f} \quad (A \gg 1),$$

so the charge gain is determined by a well-controlled component, the feedback capacitor. The signal charge Q_S will be distributed between the sensor capacitance C_{det} and the dynamic input capacitance C_i . The ratio of measured charge to signal charge

$$\frac{Q_i}{Q_s} = \frac{Q_i}{Q_{det} + Q_s} = \frac{C_i}{C_{det} + C_i} = \frac{1}{1 + \frac{C_{det}}{C_i}},$$

so the dynamic input capacitance must be large compared to the sensor capacitance.

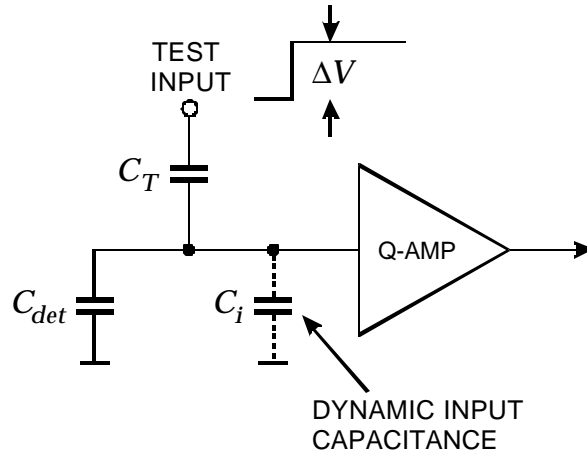


FIGURE 6. Charge calibration circuitry of a charge-sensitive amplifier

Another very useful byproduct of the integrating amplifier is the ease of charge calibration. By adding a test capacitor as shown in Fig. 6, a voltage step injects a well-

defined charge into the input node. If the dynamic input capacitance C_i is much larger than the test capacitance C_T , the voltage step at the test input will be applied nearly completely across the test capacitance C_T , thus injecting a charge $C_T \Delta V$ into the input.

Realistic Charge-Sensitive Amplifiers

The preceding discussion assumed that the amplifiers are infinitely fast, that is that they respond instantaneously to the applied signal. In reality this is not the case; charge-sensitive amplifiers often respond much more slowly than the time duration of the current pulse from the sensor. However, as shown in Fig. 7, this does not obviate the basic principle. Initially, signal charge is integrated on the sensor capacitance, as indicated by the left hand current loop. Subsequently, as the amplifier responds the signal charge is transferred to the amplifier.

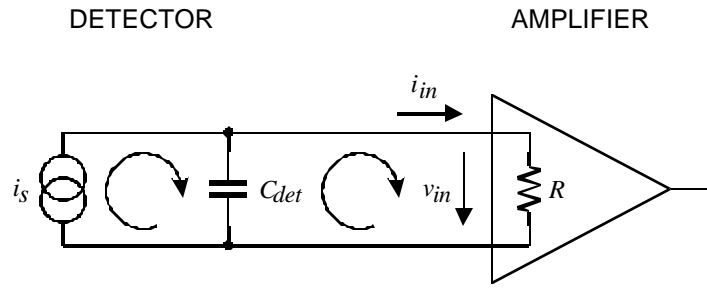


FIGURE 7. Realistic charge-sensitive amplifier

Nevertheless, the time response of the amplifier does affect the measured pulse shape. First, consider a simple amplifier as shown in Fig. 8.

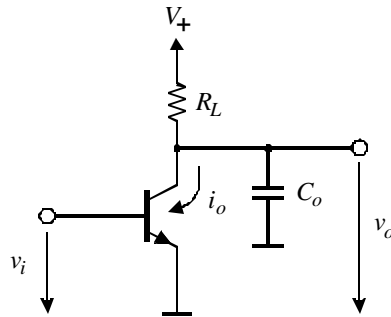


FIGURE 8. A simple amplifier

The gain element shown is a bipolar transistor, but it could also be a field effect transistor (JFET or MOSFET) or even a vacuum tube. The transistor's output current changes as the input voltage is varied. Thus, the voltage gain

$$A_V = \frac{dv_o}{dv_i} = \frac{di_o}{dv_i} \cdot Z_L \equiv g_m Z_L$$

The parameter g_m is the transconductance, a key parameter that determines gain, bandwidth and noise of transistors. The load impedance Z_L is the parallel combination of the load resistance R_L and the output capacitance C_o . This capacitance is unavoidable; every gain device has an output capacitance, the following stage has an input capacitance, and in addition the connections and additional components introduce stray capacitance. The load impedance is given by

$$\frac{1}{Z_L} = \frac{1}{R_L} + \mathbf{i}\omega C_o ,$$

where the imaginary \mathbf{i} indicates the phase shift associated with the capacitance. The voltage gain

$$A_V = g_m \left(\frac{1}{R_L} + \mathbf{i}\omega C_o \right)^{-1} .$$

At low frequencies where the second term is negligible, the gain is constant $A_V = g_m R_L$. However, at high frequencies the second term dominates and the gain falls off linearly with frequency with a 90° phase shift, as illustrated in Fig. 9. The cutoff frequency, where the asymptotic low and high frequency responses intersect, is determined by the output time constant $R_L C_o$, so the cutoff frequency

$$f_U = \frac{1}{2\pi R_L C_o} .$$

In the regime where the gain drops linearly with frequency the product of gain and frequency is constant, so the amplifier can be characterized by its gain-bandwidth product, which is equal to the frequency where the gain is one, the unity gain frequency ω_0 .

The frequency response translates into a time response. If a voltage step is applied to the input of the amplifier, the output does not respond instantaneously, as the output capacitance must first charge up. This is shown in Fig. 10.

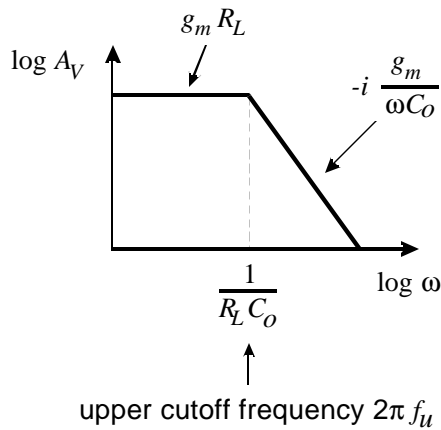


FIGURE 9. Frequency Response of a simple amplifier

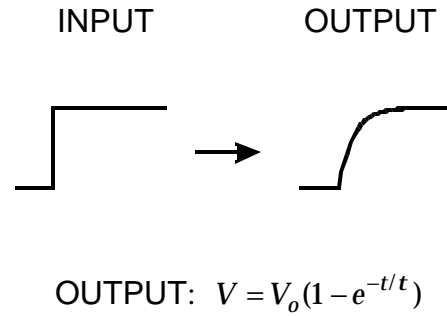


FIGURE 10. Pulse response of a simple amplifier

In practice, amplifiers utilize multiple stages, all of which contribute to the frequency response. However, for use as a feedback amplifier, only one time constant should dominate, so the other stages must have higher cutoff frequencies. Then the overall amplifier response is as shown in Fig. 9, except that at high frequencies additional corner frequencies appear.

We can now use the frequency response to calculate the input impedance and time response of a charge-sensitive amplifier. Applying the same reasoning as above, the input impedance of an amplifier as shown in Fig. 5, but with a generalized feedback impedance Z_f , is

$$Z_i = \frac{Z_f}{A+1} \approx \frac{Z_f}{A} \quad (A \gg 1)$$

At low frequencies the gain is constant and has a constant 180° phase shift, so the input impedance is of the same nature as the feedback impedance, but reduced by $1/A$. At high frequencies well beyond the amplifier's cutoff frequency f_U , the gain drops linearly with frequency with an additional 90° phase shift, so the gain

$$A = -\mathbf{i} \frac{w_0}{w}$$

In a charge-sensitive amplifier the feedback impedance

$$Z_f = -\mathbf{i} \frac{1}{wC_f},$$

so the input impedance

$$Z_i = -\frac{\mathbf{i}}{wC_f} \cdot \frac{1}{-\mathbf{i} \frac{w_0}{w}} = \frac{1}{w_0 C_f}.$$

The imaginary component vanishes, so the input impedance is real. In other words, it appears as a resistance. Thus, at low frequencies $f < f_U$ the input of a charge-sensitive amplifier appears capacitive, whereas at high frequencies $f > f_U$ it appears resistive.

Suitable amplifiers invariably have corner frequencies well below the frequencies of interest for radiation detectors, so the input impedance is resistive. This allows a simple calculation of the time response. The sensor capacitance is discharged by the resistive input impedance of the feedback amplifier with the time constant

$$t_i = R_i C_{det} = \frac{1}{w_0 C_f} \cdot C_{det}.$$

From this we see that the rise time of the charge-sensitive amplifier increases with sensor capacitance. For reasons that will become apparent later, the feedback capacitance should be much smaller than the sensor capacitance. If $C_f = C_{det}/100$, the amplifier's gain-bandwidth product must be $100/t_i$, so for a rise time constant of 10 ns the gain-bandwidth product must be 10^{10} radians = 1.6 GHz. The same result can be obtained using conventional operational amplifier feedback theory.

Apart from determining the signal rise time, the input impedance is critical in position-sensitive detectors. Fig. 11 illustrates a silicon-strip sensor read out by a bank of amplifiers. Each strip electrode has a capacitance C_{SG} to the backplane and a

fringing capacitance C_{SS} to the neighboring strips. If the amplifier has an infinite input impedance, charge induced on one strip will capacitively couple to the neighbors and the signal will be distributed over many strips (determined by C_{SS}/C_{SG}). If, on the other hand, the input impedance of the amplifier is low compared to inter-strip impedance $1/wC_{SS} \approx t_i/C_{SS}$, practically all of the charge will flow into the amplifier and the neighbors will show only a small signal.

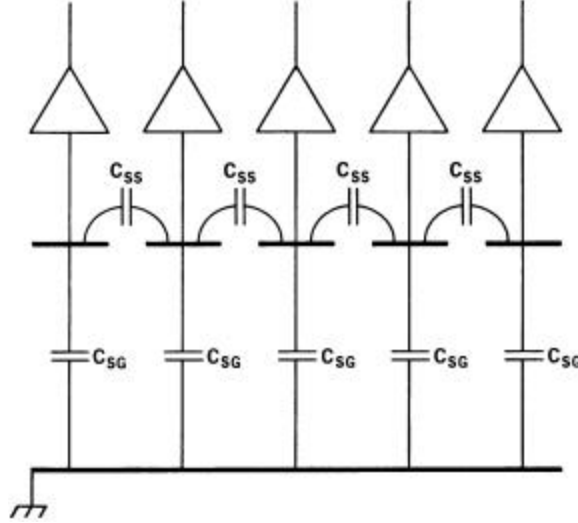


FIGURE 11. Cross coupling in a silicon strip sensor

SIGNAL PROCESSING

As noted in the introduction, one of the purposes of signal processing is to improve the signal-to-noise ratio by tailoring the spectral distributions of the signal and the electronic noise. However, for many detectors electronic noise does not determine the resolution. For example, in a NaI(Tl) scintillation detector measuring 511 keV gamma rays, say in a positron-emission tomography system, 25000 scintillation photons are produced. Because of reflective losses, about 15000 reach the photocathode. This translates to about 3000 electrons reaching the first dynode. The gain of the electron multiplier will yield about $3 \cdot 10^9$ electrons at the anode. The statistical spread of the signal is determined by the smallest number of electrons in the chain, i.e. the 3000 electrons reaching the first dynode, so the resolution $\Delta E/E = 1/\sqrt{3000} = 2\%$, which at the anode corresponds to about $5 \cdot 10^4$ electrons. This is much larger than electronic noise in any reasonably designed system. This situation is illustrated in Fig. 12 (top). In this case, signal acquisition and count rate capability may be the prime objectives of the pulse processing system. The bottom illustration in Fig. 12 shows the situation for high resolution sensors with small signals, semiconductor detectors, photodiodes or ionization chambers, for example. In this case, low noise is critical. Baseline fluctuations can have many origins, external interference, artifacts due to imperfect electronics, etc., but the fundamental limit is electronic noise.

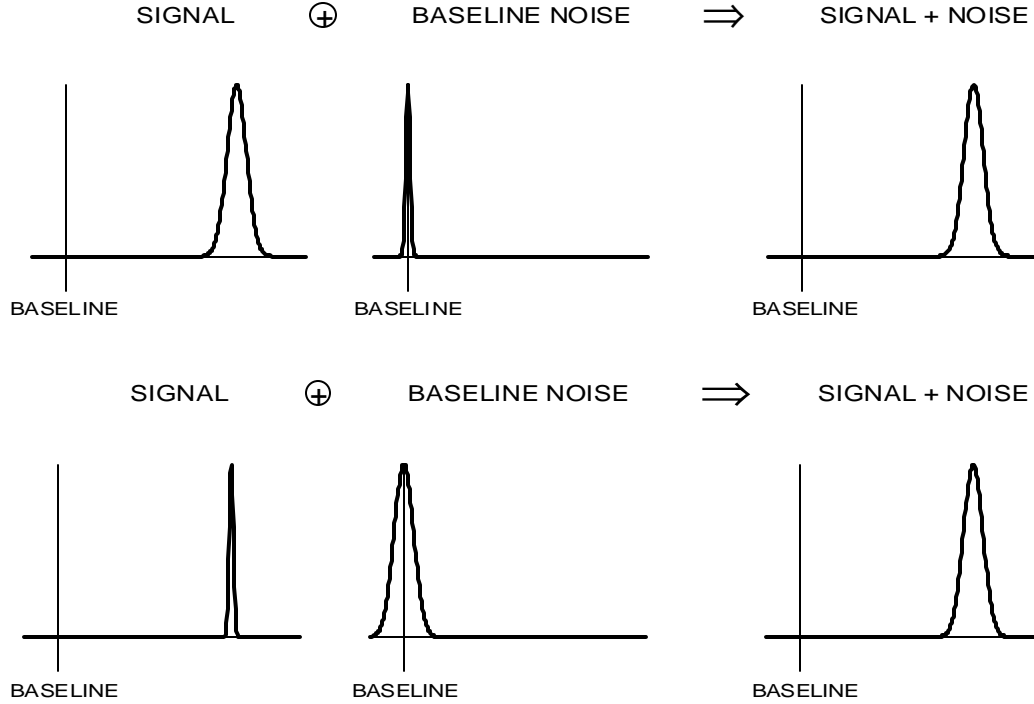


FIGURE 12. Signal and baseline fluctuations for large signal variance (top), as in scintillation detectors or proportional chambers, and for small signal variance, but large baseline fluctuations, as in semiconductor detectors or liquid Ar ionization chambers, for example.

Electronic Noise

Consider a current flowing through a sample bounded by two electrodes, i.e. n electrons moving with velocity v . The induced current depends on the spacing l between the electrodes (see “Ramo’s theorem” in ref. 7), so

$$i = \frac{nev}{l}.$$

The fluctuation of this current is given by the total differential

$$\langle di \rangle^2 = \left(\frac{ne}{l} \langle dv \rangle \right)^2 + \left(\frac{ev}{l} \langle dn \rangle \right)^2,$$

where the two terms add in quadrature, as they are statistically uncorrelated. From this one sees that two mechanisms contribute to the total noise, velocity and number fluctuations.

Velocity fluctuations originate from thermal motion. Superimposed on the average drift velocity are random velocity fluctuations due to thermal excitations. This “thermal noise” is described by the long wavelength limit of Plank’s black body spectrum where the spectral density, i.e. the power per unit bandwidth, is constant (“white” noise).

Number fluctuations occur in many circumstances. One source is carrier flow that is limited by emission over a potential barrier. Examples are thermionic emission or

current flow in a semiconductor diode. The probability of a carrier crossing the barrier is independent of any other carrier being emitted, so the individual emissions are random and not correlated. This is called “shot noise”, which also has a “white” spectrum. Another source of number fluctuations is carrier trapping. Imperfections in a crystal lattice or impurities in gases can trap charge carriers and release them after a characteristic lifetime. This leads to a frequency-dependent spectrum $dP_n/df = 1/f^\alpha$, where α is typically in the range of 0.5 to 2.

Thermal (Johnson) Noise

The most common example of noise due to velocity fluctuations is the noise of resistors. The spectral noise density vs. frequency

$$\frac{dP_n}{df} = 4kT$$

where k is the Boltzmann constant and T the absolute temperature. Since the power in a resistance R

$$P = \frac{V^2}{R} = I^2 R,$$

the spectral voltage noise density

$$\frac{dV_n^2}{df} \equiv e_n^2 = 4kTR$$

and the spectral current noise density

$$\frac{dI_n^2}{df} \equiv i_n^2 = \frac{4kT}{R}.$$

The total noise is obtained by integrating over the relevant frequency range of the system, the bandwidth. The total noise voltage at the output of an amplifier with a frequency-dependent gain $A(f)$ is

$$v_{on}^2 = \int_0^\infty e_n^2 A^2(f) df.$$

Since the spectral noise components are non-correlated (each black body excitation mode is independent), one must integrate over the noise power, i.e. the voltage squared. The total noise increases with bandwidth. Since small bandwidth corresponds to large rise-times, increasing the speed of a pulse measurement system will increase the noise. The amplitude distribution of the noise is gaussian, so noise fluctuations superimposed on the signal also yield a gaussian distribution. Thus, by measuring the width of the amplitude spectrum of a well-defined signal, one can determine the noise.

Shot Noise

The spectral noise density of shot noise is proportional to the average current

$$i_n^2 = 2q_e I,$$

where q_e is the electronic charge. Note that the criterion for shot noise is that carriers are injected independently of one another, as in thermionic or semiconductor diodes.

Current flowing through an ohmic conductor does not carry shot noise, since the fields set up by any local fluctuation in charge density can easily draw in additional carriers to equalize the disturbance.

Signal-to-Noise Ratio vs. Sensor Capacitance

The basic noise sources manifest themselves as either voltage or current fluctuations. However, the detector signal is a charge, so to allow a comparison we must express the signal as a voltage or current. This was illustrated for an ionization chamber in Fig. 5. As was noted, when the time input constant $R_{in}(C_{det} + C_{in})$ is large compared to the duration of the sensor current pulse, the signal charge is integrated on the input capacitance, yielding the signal voltage $v_S = Q_S / (C_{det} + C_{in})$. Assume that the amplifier has an input noise voltage v_n . Then the signal to noise ratio

$$\frac{v_S}{v_n} = \frac{Q_S}{v_n (C_{det} + C_{in})}.$$

This is a very important result, i.e. the signal-to-noise ratio for a given signal charge is inversely proportional to the total capacitance at the input node. Note that zero input capacitance does not yield an infinite signal-to-noise ratio. As shown in Appendix 4 of the original course notes [1], this relationship only holds for when the input time constant is greater than about ten times the sensor current pulse width. This is a general feature that is independent of amplifier type. Since feedback cannot improve signal-to-noise ratio, it also holds for charge-sensitive amplifiers, although in that configuration the charge signal is constant, but the noise increases with total input capacitance (see ref. 1). In the noise analysis the feedback capacitance adds to the total input capacitance (not the dynamic input capacitance!), so C_f should be kept small.

Pulse Shaping

Pulse shaping has two conflicting objectives. The first is to restrict the bandwidth to match the measurement time. Too large a bandwidth will increase the noise without increasing the signal. Typically, the pulse shaper transforms a narrow sensor pulse into a broader pulse with a gradually rounded maximum at the peaking time. This is illustrated in Fig. 13. The signal amplitude is measured at the peaking time T_P .

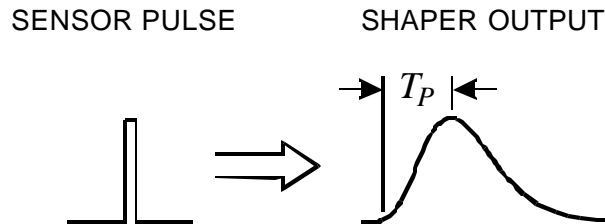


FIGURE 13. A pulse shaper transforms a short sensor pulse into a longer pulse with a rounded cusp and peaking time T_P .

The second objective is to constrain the pulse width so that successive signal pulses can be measured without overlap (pileup), as illustrated in Fig. 14. Reducing the pulse duration increases the allowable signal rate, but at the expense of electronic noise.

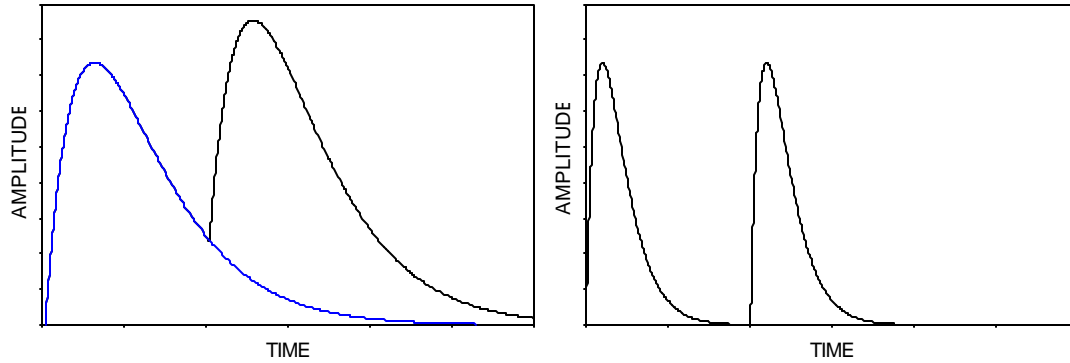


FIGURE 14. Amplitude pileup when two successive pulses overlap (left). Reducing the shaping time allows the first pulse to return to the baseline before the second arrives.

In designing the shaper it is necessary to balance these conflicting goals. Usually, many different considerations lead to a “non-textbook” compromise; “optimum shaping” depends on the application.

A simple shaper is shown in Fig. 15. A high-pass filter sets the duration of the pulse by introducing a decay time constant τ_d . Next a low-pass filter increases the rise time to limit the noise bandwidth. The high-pass is often referred to as a “differentiator”, since for short pulses it forms the derivative. Correspondingly, the low-pass is called an “integrator”. Since the high-pass filter is implemented with a CR section and the low-pass with an RC , this shaper is referred to as a CR - RC shaper. Although pulse shapers are often more sophisticated and complicated, the CR - RC shaper contains the essential features of all pulse shapers, a lower frequency bound and an upper frequency bound.

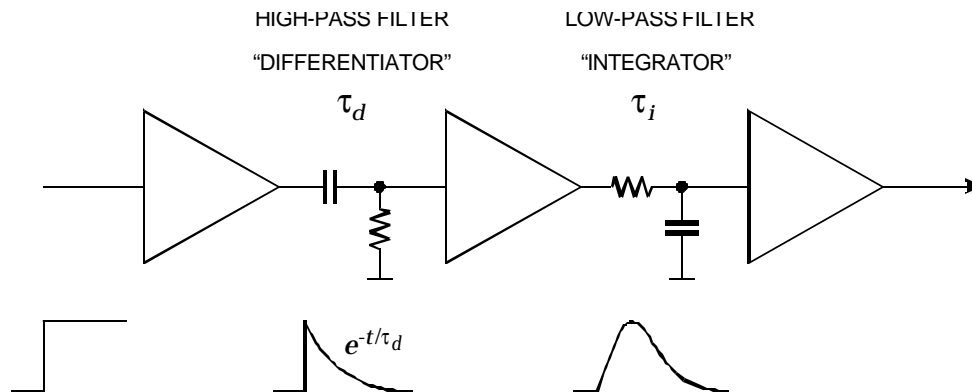


FIGURE 15. A simple pulse shaper using a CR “differentiator” as a high-pass and an RC “integrator” as a low-pass filter.

Noise Analysis of a Detector and Front-End Amplifier

To determine how the pulse shaper affects the signal-to-noise ratio consider the detector front-end in Fig. 16. The detector is represented by a capacitance, a relevant model for many radiation sensors. Sensor bias voltage is applied through the resistor R_B . The bypass capacitor C_B shunts any external interference coming through the bias supply line to ground. For high-frequency signals this capacitor appears as a low impedance, so for sensor signals the “far end” of the bias resistor is connected to ground. The coupling capacitor C_C blocks the sensor bias voltage from the amplifier input, which is why a capacitor serving this role is also called a “blocking capacitor”. The series resistance R_S represents any resistance present in the connection from the sensor to the amplifier input. This includes the resistance of the sensor electrodes, the resistance of the connecting wires or traces, any resistance used to protect the amplifier against large voltage transients (“input protection”), and parasitic resistances in the input transistor.

The following implicitly includes a constraint on the bias resistance, whose role is often misunderstood. It is often thought that the signal current generated in the sensor flows through R_b and the resulting voltage drop is measured. If the time constant $R_b C_d$ is small compared to the peaking time of the shaper T_P , the sensor will have discharged through R_b and much of the signal will be lost. Thus, we have the condition $R_b C_d \gg T_P$, or $R_b \gg T_P / C_D$. The bias resistor must be sufficiently large to block the flow of signal charge, so that all of the signal is available for the amplifier.

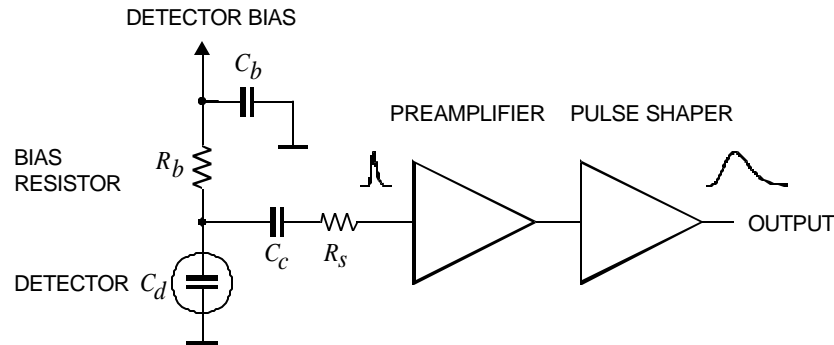


FIGURE 16. A typical detector front-end circuit

To analyze this circuit we’ll assume a voltage amplifier, so all noise contributions will be calculated as a noise voltage appearing at the amplifier input. Steps in the analysis are 1. determine the frequency distribution of all noise voltages presented to the amplifier input from all individual noise sources, 2. integrate over the frequency response of the shaper (for simplicity a CR - RC shaper) and determine the total noise voltage at the shaper output, and 3. determine the output signal for a known input signal charge. The equivalent noise charge (ENC) is the signal charge for $S/N = 1$.

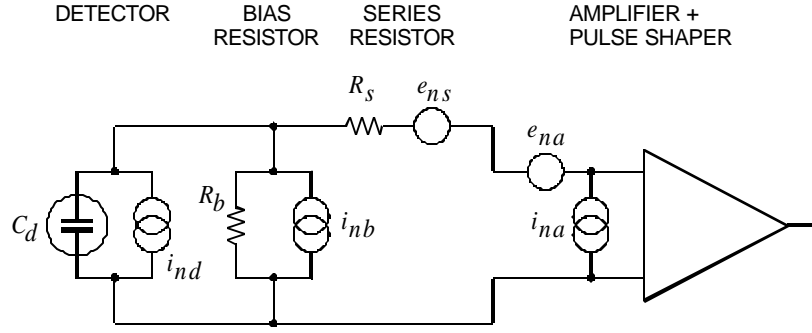


FIGURE 17. Equivalent circuit of a detector front-end for noise analysis.

The equivalent circuit for the noise analysis (Fig. 17) includes both current and voltage noise sources. The “shot noise” i_{nd} of the sensor leakage current is represented by a current noise generator in parallel with the sensor capacitance. As noted above, resistors can be modeled either as a voltage or current generator. Generally, resistors shunting the input act as noise current sources and resistors in series with the input act as noise voltage sources (which is why some in the detector community refer to current and voltage noise as “parallel” and “series” noise). Since the bias resistor effectively shunts the input, as the capacitor C_b passes current fluctuations to ground, it acts as a current generator i_{nb} and its noise current has the same effect as the shot noise current from the detector. By the way, one can also model the shunt resistor as a noise voltage source and obtain the result that it acts as a current source. Choosing the appropriate model merely simplifies the calculation. Any other shunt resistances can be incorporated in the same way. Conversely, the series resistor R_s acts as a voltage generator. The electronic noise of the amplifier is described fully by a combination of voltage and current sources at its input, shown as e_{na} and i_{na} .

Thus, the noise sources are

$$\text{sensor bias current: } i_{nd}^2 = 2q_e I_d$$

$$\text{shunt resistance: } i_{nb}^2 = \frac{4kT}{R_b}$$

$$\text{series resistance: } e_{ns}^2 = 4kTR_s$$

where q_e is the electronic charge, I_d the sensor bias current, k the Boltzmann constant and T the temperature. Typical amplifier noise parameters e_{na} and i_{na} are of order $\text{nV}/\sqrt{\text{Hz}}$ and $\text{pA}/\sqrt{\text{Hz}}$. Amplifiers tend to exhibit a “white” noise spectrum at high frequencies (greater than order kHz), but at low frequencies show excess noise components with the spectral density

$$e_{nf}^2 = \frac{A_f}{f}$$

where the noise coefficient A_f is device specific and of order $10^{-10} - 10^{-12} \text{ V}^2$.

The noise voltage generators are in series and simply add in quadrature. White noise distributions remain white. However, a portion of the noise currents flows

through the detector capacitance, resulting in a frequency-dependent noise voltage $i_n / (\omega C_d)$, so the originally white spectrum of the sensor shot noise and the bias resistor now acquires a $1/f$ behavior. The frequency distribution of all noise sources is further altered by the combined frequency response of the amplifier chain $A(f)$. Integrating over the cumulative noise spectrum at the amplifier and comparing to the output for a known input signal yields the signal-to-noise ratio. In this example the shaper is a simple CR - RC shaper, where for a given differentiation time constant, minimum noise obtains when the differentiation and integration time constants are equal $t_i = t_d \equiv t$. In this case the output pulse assumes its maximum amplitude at the time $T_P = t$.

Although the basic noise sources are currents or voltages, since radiation detectors are typically used to measure charge, the system's noise level is conveniently expressed as an equivalent noise charge Q_n . As noted previously, this is equal to the detector signal that yields a signal-to-noise ratio of one. The equivalent noise charge is commonly expressed in Coulombs, the corresponding number of electrons, or the equivalent deposited energy (eV). For the above circuit the equivalent noise charge

$$Q_n^2 = \left(\frac{e^2}{8} \right) \left[\left(2q_e I_d + \frac{4kT}{R_b} + i_{na}^2 \right) \cdot t + \left(4kTR_S + e_{na}^2 \right) \cdot \frac{C_d^2}{t} + 4A_f C_d^2 \right]$$

The prefactor $(e^2/8)$ normalizes the noise to the signal gain. The first term combines all noise current sources and increases with shaping time. The second term combines all noise voltage sources and decreases with shaping time, but increases with sensor capacitance. The third term is the contribution of excess $(1/f)$ noise and, as a voltage source, also increases with sensor capacitance. The $1/f$ term is independent of shaping time, since for a $1/f$ spectrum the total noise depends on the ratio of upper to lower cutoff frequency, which depends only on shaper topology, but not on the shaping time.

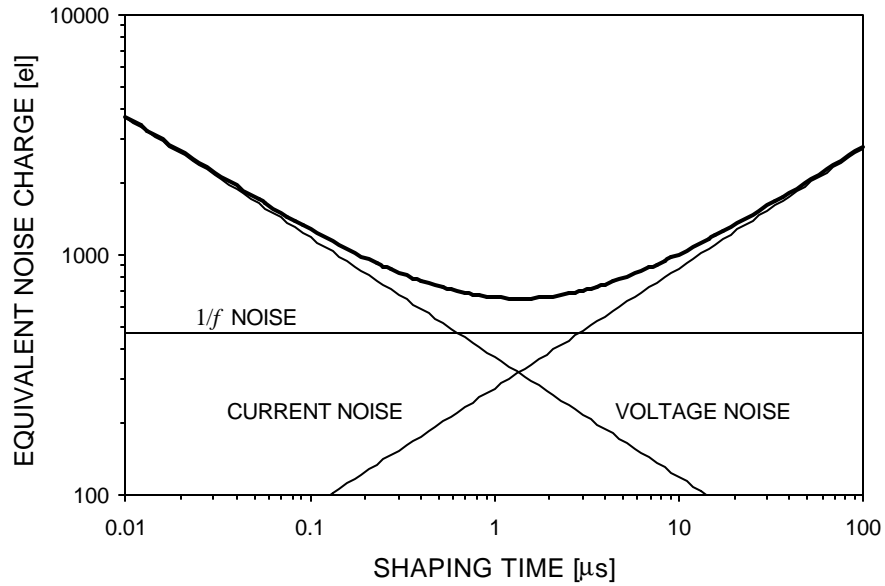


FIGURE 18. Equivalent noise charge vs. shaping time

Fig. 18 shows how ENC is affected by shaping time. At short shaping times the voltage noise dominates, whereas at long shaping times the current noise takes over. Minimum noise obtains where the current and voltage contributions are equal. The noise minimum is flattened by the presence of $1/f$ noise. Increasing the detector capacitance will increase the voltage noise contribution and shift the noise minimum to longer shaping times.

For quick estimates one can use the following equation, which assumes an FET amplifier (negligible i_{na}) and a simple CR - RC shaper with peaking time t .

$$Q_n^2 = 12 \left[\frac{e^2}{\text{nA} \cdot \text{ns}} \right] I_d t + 6 \cdot 10^5 \left[\frac{e^2 \text{ k}\Omega}{\text{ns}} \right] \frac{t}{R_b} + 3.6 \cdot 10^4 \left[\frac{e^2 \text{ ns}}{(\text{pF})^2 (\text{nV})^2 / \text{Hz}} \right] e_n^2 \frac{C^2}{t}$$

After peaking the output of a simple CR - RC shaper returns to baseline rather slowly. The pulse can be made more symmetrical, allowing higher signal rates for the same peaking time. Very sophisticated circuits have been developed to improve this situation, but a conceptually simple way is to use multiple integrators, as illustrated in Fig. 19. In this case the integration time constant is made smaller than the differentiation time constant to maintain the peaking time. Note that the peaking time is a key design parameter, as it dominates the noise bandwidth and must also accommodate the sensor response time.

Another type of shaper is the correlated double sampler, illustrated in Fig. 20. This type of shaper is widely used in monolithically integrated circuits, as many CMOS processes provide only capacitors and switches, but no resistors. Input signals are superimposed on a slowly fluctuating baseline. To remove the baseline fluctuations the baseline is sampled prior to the signal. Next, the signal plus baseline is sampled and the previous baseline sample subtracted to obtain the signal. The prefilter is critical to limit the noise bandwidth of the system. Filtering after the sampler is

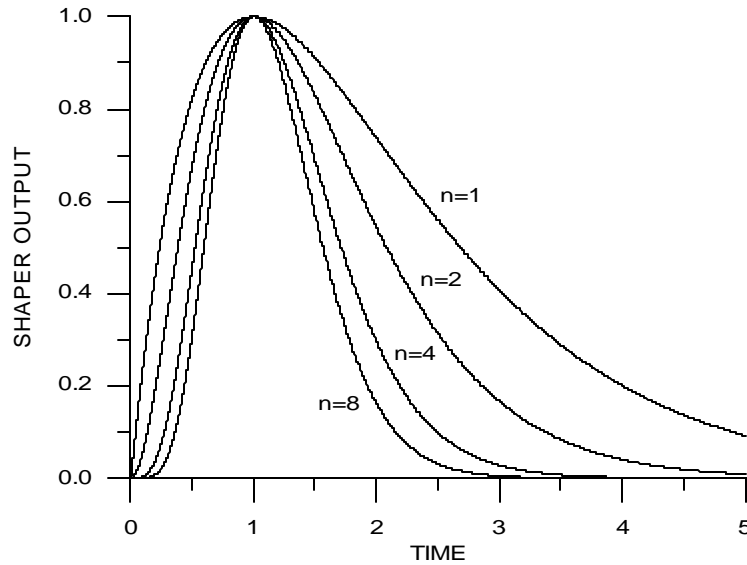


FIGURE 19. Pulse shape vs. number of integrators in a CR - nRC shaper

useless, as noise fluctuations on time scales shorter than the sample time will not be removed. Here the sequence of filtering is critical, unlike a time-invariant linear filter where the sequence of filter functions can be interchanged.

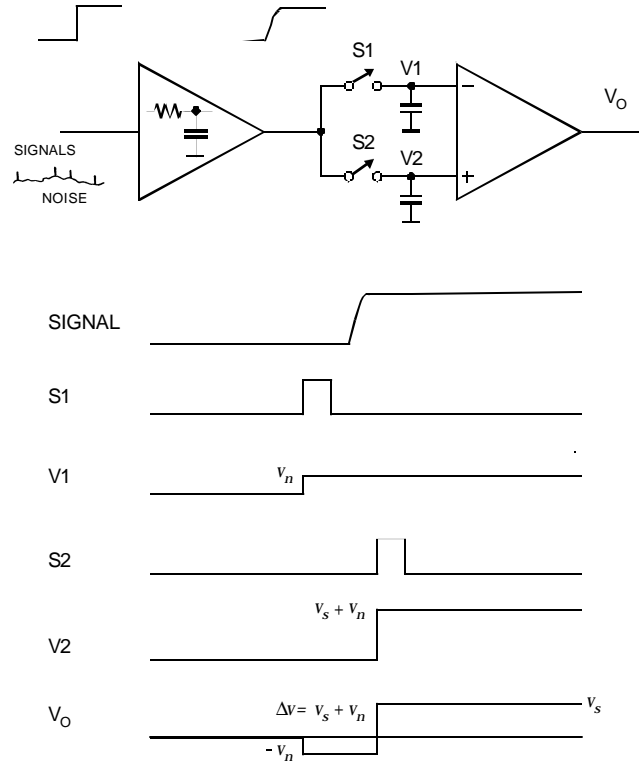


FIGURE 20. Principle of a correlated double sample shaper

This is an example of a time-variant filter. The $CR-nRC$ filter described above acts continuously on the signal, whereas the correlated double sample changes filter parameters vs. time. Time-variant filters cannot be analyzed in the frequency domain (except for some special cases that can be analyzed by analogy). However, just as filter response can be described either in the frequency or time domain, so can the noise performance. This is explained in more detail in refs. 3 through 6. The key is Parseval's theorem

$$\int_0^{\infty} |A(f)|^2 df = \int_{-\infty}^{\infty} [F(t)]^2 dt .$$

The left hand side is essentially integration over the noise bandwidth. The output noise power scales linearly with the duration of the pulse, so the noise contribution of the shaper can be split into a factor that is determined by the shape of the response and a time factor that sets the shaping time. This leads to a general formulation of the equivalent noise charge

$$Q_n^2 = i_n^2 F_i T_S + e_n^2 F_v \frac{C^2}{T_S} + F_v A_f C^2 ,$$

where C is the sum of all capacitances shunting the input, F_i , F_v and F_{vf} depend on the shape of the pulse determined by the shaper and T_S is a characteristic time, for example the peaking time of a CR - nRC shaped pulse or the sampling interval in a correlated double sampler. The shape factors F_i , F_v are easily calculated

$$F_i = \frac{1}{2T_S} \int_{-\infty}^{\infty} [W(t)]^2 dt, \quad F_v = \frac{T_S}{2} \int_{-\infty}^{\infty} \left[\frac{dW(t)}{dt} \right]^2 dt.$$

For time-invariant pulse shaping $W(t)$ is simply the system's impulse response (the output signal seen on an oscilloscope) with the peak output signal normalized to unity. For a time-variant shaper the same equations apply, but the shape factors are determined differently. See references [3] through [6] for more details.

A pulse shaper formed by a single differentiator and integrator with equal time constants has $F_i = F_v = 0.9$ and $F_{vf} = 4$, independent of the shaping time constant, so for the circuit in Fig. 16

$$Q_n^2 = \left(2q_e I_d + \frac{4kT}{R_b} + i_{na}^2 \right) F_i T_S + \left(4kTR_s + e_{na}^2 \right) F_v \frac{C_d^2}{T_S} + F_{vf} A_f C_d^2.$$

Pulse shapers can be designed to reduce the effect of current noise, e.g. mitigate radiation damage. Increasing pulse symmetry tends to decrease F_i and increase F_v , e.g. to $F_i = 0.45$ and $F_v = 1.0$ for a shaper with one CR differentiator and four cascaded RC integrators.

Noise is improved by reducing the detector capacitance and leakage current, judiciously selecting all resistances in the input circuit, and choosing the optimum shaping time constant. The noise parameters of a well-designed amplifier depend primarily on the input device. Fast, high-gain transistors are generally best.

In field effect transistors, both junction field effect transistors (JFETs) or metal oxide silicon field effect transistors (MOSFETs), the noise current contribution is very small, so reducing the detector leakage current and increasing the bias resistance will allow long shaping times with correspondingly lower noise. The equivalent input noise voltage $e_n^2 \approx 4kT / g_m$, where g_m is the transconductance, which increases with operating current. For a given current, the transconductance increases when the channel length is reduced, so reductions in feature size with new process technologies are beneficial. At a given channel length minimum noise obtains when a device is operated at maximum transconductance. If lower noise is required, the width of the device can be increased (equivalent to connecting multiple devices in parallel). This increases the transconductance (and required current), but also increases the input capacitance. At some point the reduction in noise voltage is outweighed by the increase in total input capacitance. The optimum obtains when the FET's input capacitance equals the external capacitance (sensor + stray capacitance). Note that this capacitive matching criterion only applies when the input current noise contribution of the amplifying device is negligible.

Capacitive matching comes at the expense of power dissipation. Since the minimum is shallow, one can operate at significantly lower currents with just a minor increase in noise. In large detector arrays power dissipation is critical, so FETs are hardly ever operated at their minimum noise. Instead, one seeks an acceptable compromise between noise and power dissipation. Similarly, the choice of input devices is frequently driven by available fabrication processes. High-density

integrated circuits tend to include only CMOS devices, so this determines the input device, even where a bipolar transistor would provide better performance.

In bipolar transistors the shot noise associated with the base current I_b is significant, $i_{nb}^2 = 2q_e I_b$. Since $I_b = I_c / b_{DC}$, where I_c is the collector current and b_{DC} the DC current gain, this contribution increases with device current. On the other hand, the equivalent input noise voltage

$$e_n^2 = \frac{2(kT)^2}{q_e I_c}$$

decreases with collector current, so the noise assumes a minimum at a specific collector current.

$$Q_{n,\min}^2 = 4kT \frac{C}{\sqrt{b_{DC}}} \sqrt{F_i F_v} \quad \text{at} \quad I_c = \frac{kT}{q_e} C \sqrt{b_{DC}} \sqrt{\frac{F_v}{F_i}} \frac{1}{T_s}$$

For a CR-RC shaper

$$Q_{n,\min} \approx 800 \left[\frac{e}{\sqrt{\text{pF}}} \right] \cdot \frac{\sqrt{C}}{\sqrt[4]{b_{DC}}}.$$

The minimum obtainable noise is independent of shaping time (unlike FETs), but only at the optimum collector current I_c , which does depend on shaping time.

In bipolar transistors the input capacitance is usually much smaller than the sensor capacitance (of order 1 pF), substantially smaller than in FETs with comparable noise. Since the transistor input capacitance enters into the total input capacitance, this is an advantage. Note that capacitive matching does not apply to bipolar transistors. Due to the base current noise bipolar transistors are best at short shaping times, where they also require lower power than FETs for a given noise level.

When the input noise current is negligible, the noise increases linearly with sensor capacitance. The noise slope

$$\frac{dQ_n}{dC_d} \approx 2e_n \cdot \sqrt{\frac{F_v}{T}}$$

depends both on the preamplifier (e_n) and the shaper (F_v, T). The zero intercept can be used to determine the amplifier input capacitance plus any additional capacitance at the input node

$$Q_n|_{C_d=0} = (C_{amp} + C_{stray}) \cdot e_n \sqrt{\frac{F_v}{T}}.$$

Practical noise levels range from <1 e for CCDs at long shaping times to $\sim 10^4$ e in high-capacitance liquid Ar calorimeters. Silicon strip detectors typically operate at $\sim 10^3$ electrons, whereas pixel detectors with fast readout provide noise of several hundred electrons. Transistor noise is discussed in more detail in [7].

Timing Measurements

In timing measurements the slope-to-noise ratio must be optimized, rather than the signal-to-noise ratio alone, so the rise time t_r of the pulse is important. The “jitter” S_t of the timing distribution

$$S_t = \frac{S_n}{(dS/dt)_{S_T}} \approx \frac{t_r}{S/N}$$

where S_n is the rms noise and the derivative of the signal dS/dt is evaluated at the trigger level S_T . To increase dS/dt without incurring excessive noise the amplifier bandwidth should match the rise-time of the detector signal. The 10 to 90% rise time of an amplifier with bandwidth f_u (see Fig. 9) is

$$t_r = 2.2 t = \frac{2.2}{2p f_u} = \frac{0.35}{f_u}$$

For example, an oscilloscope with 350 MHz bandwidth has a 1 ns rise time. When amplifiers are cascaded, which is invariably necessary, the individual rise times add in quadrature

$$t_r \approx \sqrt{t_{r1}^2 + t_{r2}^2 + \dots + t_{rm}^2}$$

Increasing signal-to-noise ratio also improves time resolution, so minimizing the total capacitance at the input is also important. At high signal-to-noise ratios the time jitter can be much smaller than the rise time. The timing distribution may shift with signal level (“walk”), but this can be corrected by various means, either in hardware or software. For a more detailed tutorial on timing measurements see ref. [8].

INTERFERENCE AND PICKUP

The previous discussion analyzed random noise sources inherent to the sensor and front-end electronics. In practical systems external noise often limits the obtainable detection threshold or energy resolution. As with random noise, external pickup introduces baseline fluctuations. There are many possible sources, radio and television stations, local RF generators, system clocks, transients associated with trigger signal and data readout, etc. Furthermore, there are many ways through which these undesired signals can enter the system. Again, a comprehensive review exceeds the allotted space, so only a few key examples of pickup mechanisms will be shown. A more detailed discussion is in the course notes [1].

The most sensitive node is the input. Fig. 21 shows how very small spurious signals coupled to the sensor backplane can inject substantial charge. Any change in the bias voltage ΔV directly at the sensor backplane will inject a charge $\Delta Q = C_{det} \Delta V$. Assume a silicon strip sensor with 10 cm strip length. Then C_{det} for a single strip is about 10 pF. If the noise level is $Q_n = 1000$ electrons ($1.6 \cdot 10^{-16}$ C), ΔV must be much smaller than $Q_n / C_{det} = 16 \mu V$. This can be introduced as noise from the bias supply (some voltage supplies are quite noisy; switching power supplies can be clean, but most aren't) or noise on the ground plane can couple through the capacitor C . Naively,

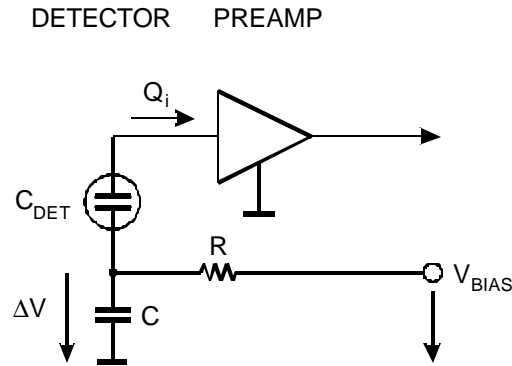


FIGURE 21. Spurious charge injection through the sensor.

one might assume the ground plane to be “clean”, but it can carry significant interference for the following reason.

One of the most common mechanisms for cross-coupling is shared current paths, often referred to as “ground loops”. However, this phenomenon is not limited to grounding. Consider two systems. The first is transmitting large currents from a source to a receiver. The second is similar, but is attempting a low-level measurement. According to the prevailing lore, both systems are connected to a massive ground bus, as shown in Fig. 22. Current seeks the path of least resistance, so the large current from source V_1 will also flow through the ground bus. Although the ground bus is massive, it does not have zero resistance, so the large current flowing through the ground system causes a voltage drop ΔV .

In system 2 (source V_2) both signal source and receiver are also connected to the ground system. Now the voltage drop ΔV from system 1 is in series with the signal path, so the receiver measures $V_2 + \Delta V$. The cross-coupling has nothing to do with grounding *per se*, but is due to the common return path. However, the common ground caused the problem by establishing the shared path. This mechanism is not

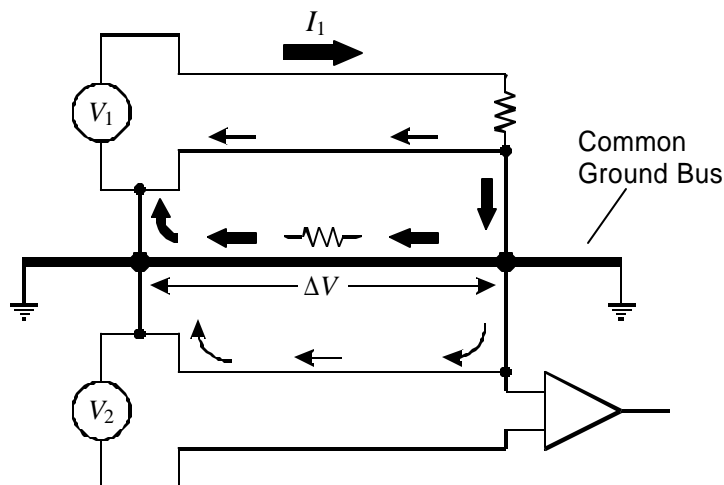


FIGURE 22. Shared current paths among grounded systems.

limited to large systems with external ground busses, but also occurs on the scale of printed circuit boards and micron-scale integrated circuits. At high frequencies the impedance is increased due to skin effect and inductance. Note that for high-frequency signals the connections can be made capacitively, so even if there is no DC path, the parasitic capacitance due to mounting structures or adjacent conductor planes can be sufficient to close the loop.

The traditional way of dealing with this problem is to reduce the impedance of the shared path, which leads to the “copper braid syndrome”. However, changes in the system will often change the current paths, so this “fix” is not very reliable. Furthermore, in many detector systems – tracking detectors, for example – the additional material would be prohibitive. Instead, it is best to avoid the root cause. Fig. 23 shows a sensor connected to a multistage amplifier. Signals are transferred from stage to stage through definite current paths. It is critical to maintain the integrity of the signal paths, but this does not depend on grounding – indeed Fig. 23 does not show any ground connection at all. The most critical parts of this chain are the input, which is the most sensitive node, and the output driver, which tends to circulate the largest current. Circuit diagrams usually are not drawn like Fig. 23; the bottom common line

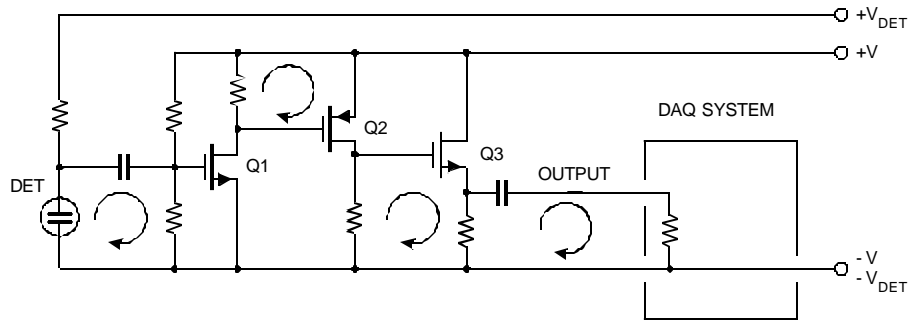


FIGURE 23. Local signal current return paths in a sensor and amplifier.

is typically shown as ground. For example, in Fig. 21 the sensor signal current flows through capacitor C and reaches the return node of the amplifier through “ground”. Clearly, it is critical to control this path and keep deleterious currents from this area.

However superfluous grounding may be, one cannot let circuit elements simply float with respect to their environment. Capacitive coupling is always present and any capacitive coupling between two points of different potential will induce a signal. This is illustrated in Fig. 24, which represents individual detector modules mounted on a support/cooling structure. Interference can couple through the parasitic capacitance of the mount, so it is crucial to reduce the capacitance and control the potential of the support structure relative to the detector module. Attaining this goal in reality is a challenge, which is not always met successfully. Nevertheless, paying attention to signal paths and potential references early on is much easier than attempting to correct a poor design after it’s done. Troubleshooting is exacerbated by the fact that current paths interact, so doing the “wrong” thing sometimes brings improvement. Furthermore, only one mistake can ruin system performance, so if this has been designed into the system from the outset, one is left with compromises. Nevertheless, although this area is rife with myths, basic physics still applies.

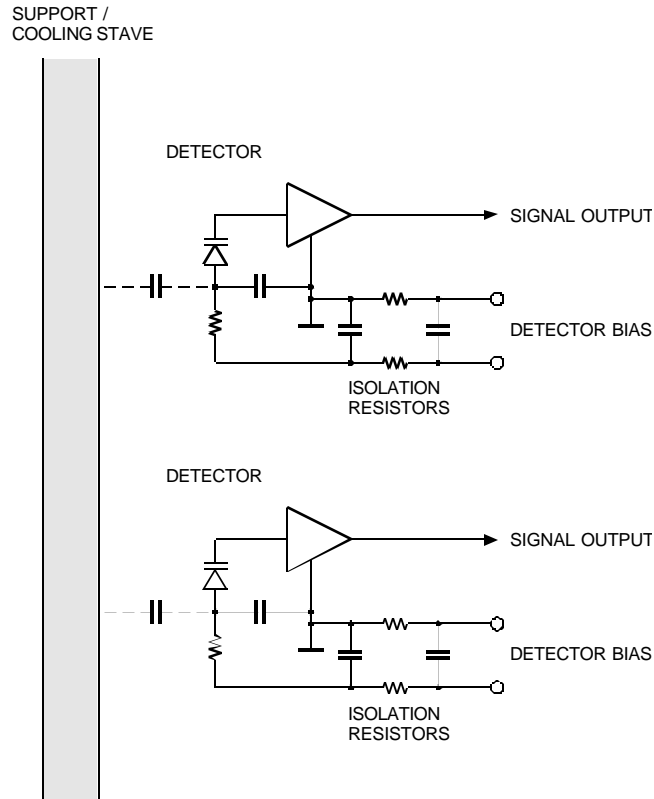


FIGURE 24. Pickup through mounting structures

CONCLUSION

Signal processing is a key part of modern detector systems. Proper design is especially important when signals are small and electronic noise determines detection thresholds or resolution. Optimization of noise is well understood and predicted noise levels can be achieved in practical experiments within a few percent of predicted values. However, systems must be designed very carefully to avoid extraneous pickup.

This work was supported by the Director, Office of Science, Office of High Energy and Nuclear Physics, of the U.S. Department of Energy under Contract No. DE-AC03-76SF00098

REFERENCES

1. http://www-physics.lbl.gov/~spieler/ICFA_Morelia/index.html
2. <http://www-physics.lbl.gov/~spieler>
3. Radeka, V., Nucl. Instr. and Meth. **99**, 525 (1972).
4. Radeka, V., IEEE Trans. Nucl. Sci. **NS-21**, 51 (1974).
5. Goulding, F.S., Nucl. Instr. and Meth. **100**, 493 (1972).
6. Goulding, F.S., IEEE Trans. Nucl. Sci. **NS-29**, 1125-1142 (1982).
7. http://www-physics.lbl.gov/~spieler/Heidelberg_Notes/index.html
8. Spieler, H., IEEE Trans. Nucl. Sci. **NS-29**, 1142-1158 (1982).